Electronic Supplementary Information for: Alkaline manganese electrochemistry studied by in situ and operando spectropscopic methods - metal dissolution, oxide formation and oxygen evolution

Martin Rabe Cigdem Toparli Ying-Hsuan Chen Olga Kasian
Karl J.J. Mayrhofer Andreas Erbe

1 Thermodynamic data

To obtain an overview of the thermodynamics of the system investigated, the freely available programme MEDUSA with its native HYDRA database was used to calculate predominance area diagrams.[1] MEDUSA works by implementing established algorithms.[2–4] In the calculation, 29 species were included, including 7 solid species. The latter were Mn, MnO, $Mn(OH)_2$, α-MnOOH, Mn_3O_4, Mn_2O_3, MnO_2. Manganese hydride species were not included. Some of the resulting diagrams are shown in ESI-Fig. 1.

For comparison with experimental data, it is most relevant to analyse the predominance diagram in the form of electrode potential vs. total dissolved concentration of manganese species, $[Mn]_{tot}$, at fixed pH=13, as given in ESI-Fig. 1a. From the diagram, we obtain the following electrode potentials for transitions between the solid manganese hydroxides and oxides: $Mn(OH)_2 \longrightarrow Mn_3O_4$ at -0.306 V_{SHE} (-0.516 $V_{Ag|AgCl}$), $Mn_3O_4 \longrightarrow Mn_2O_3$ at +0.062 V_{SHE} (-0.148 $V_{Ag|AgCl}$), $Mn_2O_3 \longrightarrow MnO_2$ at +0.206 V_{SHE} (-0.004 $V_{Ag|AgCl}$), and dissolution of MnO_2 to MnO_4^- above +0.450 V_{SHE} (0.24 $V_{Ag|AgCl}$) for activity $[Mn]_{tot} = 10^{-10}$.

For two activities of totally dissolved Mn, the potential-pH diagrams are given in ESI-Fig. 1b and c, as the pH at the electrode surface is likely higher after polarising to the most negative potentials in the experiments for this work. These diagrams manifest a certain solubility of the amorphous $Mn(OH)_2$ which is supposed to cover the manganese surface in aqueous solutions.

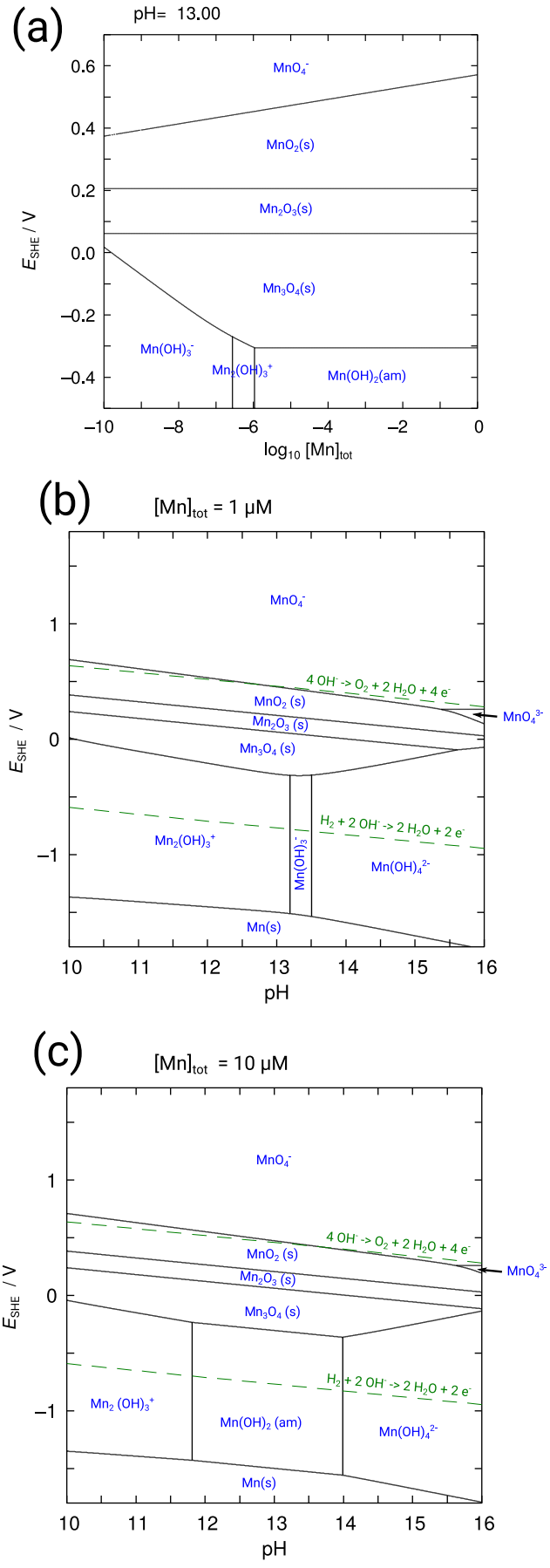

ESI-Fig. 1: (a) Predominance area diagrams for Mn at pH=13. (b) and (c) shows predominance areas diagrams in the form of potential-pH diagrams for Mn at alkaline pH for two different concentration of dissolved Mn species $[\mathrm{Mn}]_{\mathrm{tot}}$ as indicated in the graph.

2 Calibration data to obtain thickness values from ellipsometric spectra

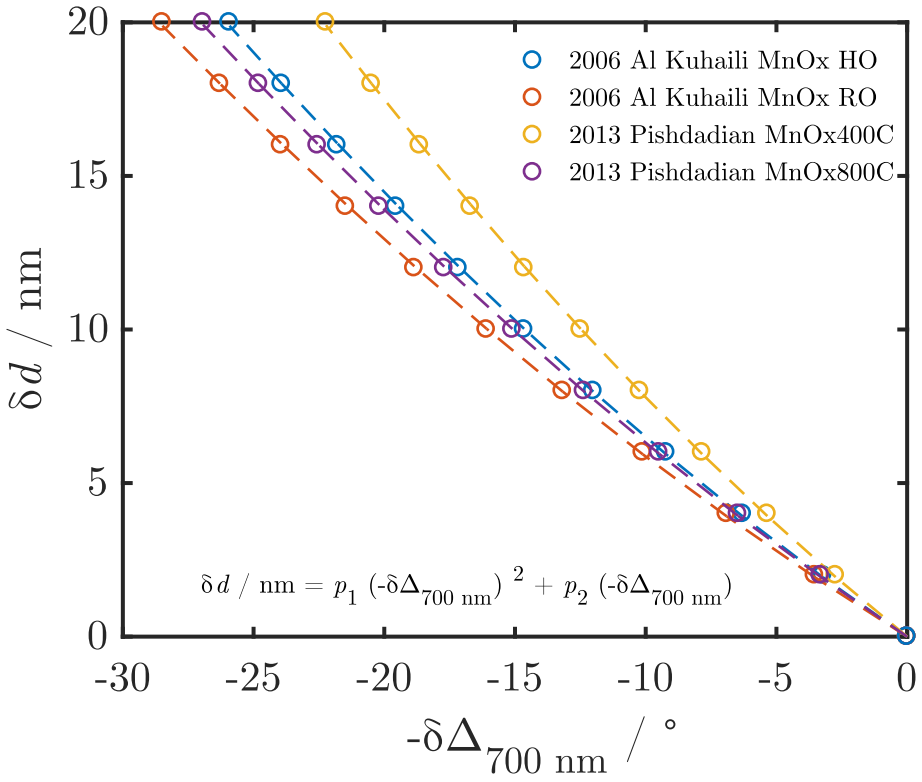

ESI-Fig. 2: Thickness calibration data. Δ was calculated for different oxide layer thicknesses δd as described in detail in the main part experimental section 2.3. Calibration was obtained by fitting the 2nd degree polynomial stated. The fitted parameters and are given in ESI-Table 1.

ESI-Table 1: Fit results for δd calibration.

n, k source	$p_1/10^{-3}$	p_2
MnOx HO[5]	7.39	-0.576
MnOx RO[5]	6.06	-0.526
MnOx 400C[6]	9.55	-0.683
MnOx 800C[6]	6.43	-0.566

3 Voltammogram with extended potential range

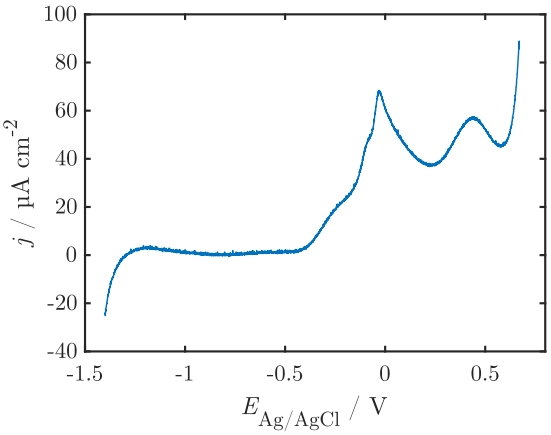

ESI-Fig. 3: First anodic scan in CV of Mn in NaOH (0.1 M) at 2 mV / s. Sharp current de-/increase below −1.3 V and above 0.6 V indicate the onsets of the hydrogen evolution reaction (HER) and oxygen evolution reaction (OER), respectively.

4 Overview over assignment of peaks observed in the Raman spectra

ESI-Table 2: Raman peaks of Mn oxides observed in situ in this work, with possible assignment and in relation to literature

Compound	Peak / cm^{-1}	Lit. Peak / cm^{-1}	Mode	Ref.
MnO		530	LO	[7, 8]
Mn_3O_4	505-508	506		[9]
Mn_3O_4		575		[9]
Mn_3O_4		657		[10]
Mn_3O_4		660	2TO	[7]
Mn_3O_4		730	2TO	[7]
α-Mn_2O_3	402-406	396		[10]
α-Mn_2O_3		690		[10]
α-MnO_2	588-592	574	A_g	[10]
α-MnO_2	626-629	634	A_g	[10]
α-MnO_2	468-475		[IR active]	[9]
β-MnO_2		750	B_{2g}	[10, 11]
β-MnO_2		538	E_g	[9, 10, 12]
β-MnO_2		162	B_{1g}	[10]
β-MnO_2		667	A_{1g}	[9–11]

5 Ex-situ analysis by X-ray photoelectron spectroscopy (XPS)

5.1 Experimental

The manganese oxidation was studied by XPS using monochromated Al Kα 1486.6 eV X-rays. After sample preparation by PVD, depth profiles of Mn samples were recorded by XPS. For sputtering an Ar^+ ion beam with an energy of 1 kV on an area of 2 mm × 2 mm and an etching time of 60 s per step was used. For depth profiling spectra were recorded with a pass energy of 26 eV and a step size of 0.1 eV. The takeoff angle was 45°. Furthermore, two samples were investigated after CV and CA experiment, using a pass energy of 50 eV, and 0.1 eV step size. Binding energies were calibrated by positioning the main C 1s peak at 284.8 eV.

5.2 Results of Mn oxidation state determination

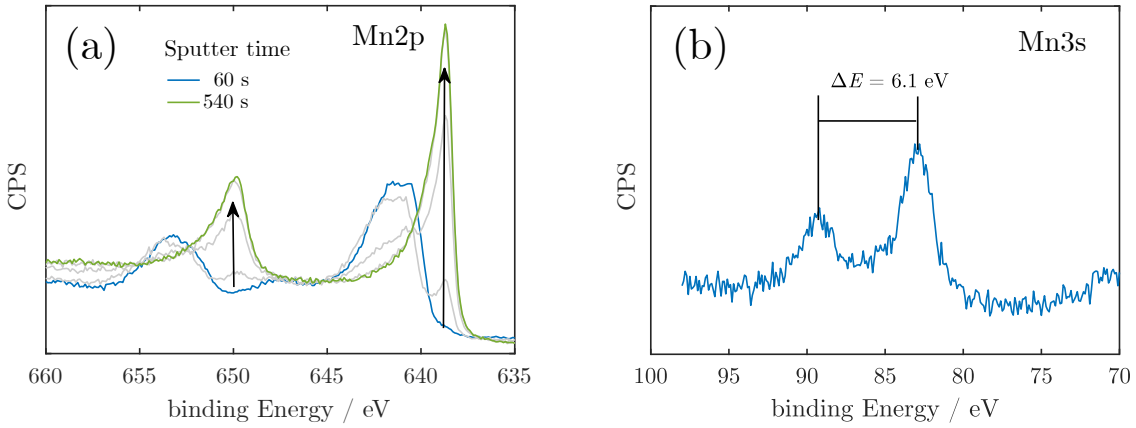

ESI-Fig. 4: XPS spectra of a freshly prepared Mn surface. (a) Mn 2p spectra with interleaved sputtering cycles (2 min per spectrum). Evolving Mn metal peaks at 638.7 eV and 649.9 eV prove the existence of bare metal under thin native oxide layer; (b) Mn 3s spectrum of native Mn oxide.

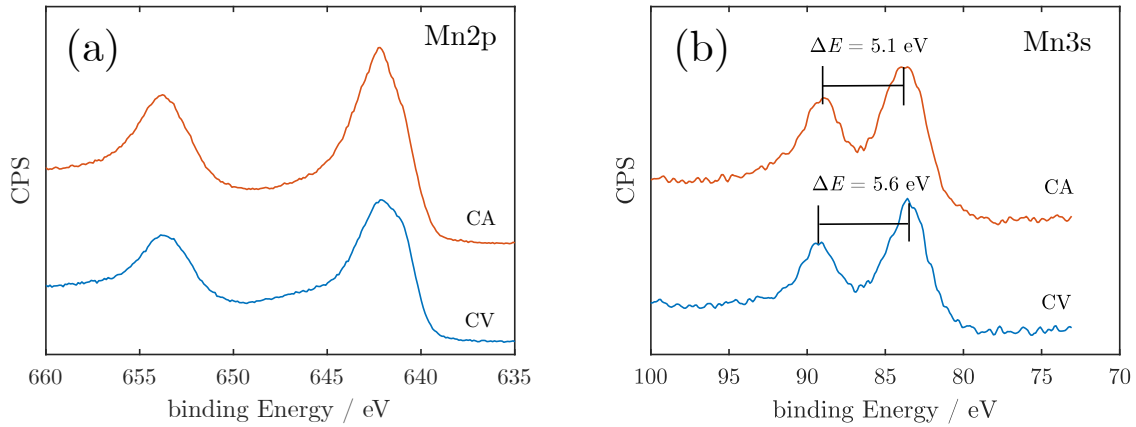

ESI-Fig. 5: Ex situ XPS spectra of surfaces after CV and CA experiments. (a) Mn 2p spectra; (b) Mn 3s spectra.

XPS was employed to investigate changes in the manganese oxidation state by monitoring the binding energy shift, satellite peak splitting, and exchange peak splitting for the Mn 2p and 3s peaks. These parameters for control manganese oxides samples are well documented in the literature.[13–15]

During PVD substantial amount of manganese oxide originating from the source metal may precipitate on the sample. Thus as a control depth profiles of the freshly prepared Mn samples were measured (ESI-Fig. 4). The Mn 2p signal splits into two peaks due to spin-orbit splitting. The Mn 2p spectra at short sputtering times, i.e. close to the interface are dominated by relatively broad peaks at 641.2 and 653.2 eV indicating that native oxide formed directly on the sample in contact with air (ESI-Fig. 4a). With increasing sputtering time two peaks at 638.7 and 649.9 eV grow, indicating that the bare metal is reached below the thin native oxide layer.[16]. A reliable diagnostic for Mn oxidation state is the degree of Mn 3s peak splitting that is caused primarily by the exchange interaction between the 3s and 3d electrons.[17] The Mn 3s spectrum of the native oxide show a splitting of 6.1 eV, which indicates the dominance of Mn^{II}, e.g. in the form of MnO.[18]

Two samples were investigated after in situ CV and CA experiments (ESI-Fig. 5). Mn 2p core level spectrum of the sample measured after CV and CA experiment displays two peaks at binding energies of 653.8 eV and 642 eV with a spin-orbit separation of 11.8 eV. These results are in accordance with the reported data of Mn $2p_{3/2}$ and Mn $2p_{1/2}$ for Mn_3O_4.[19, 20] The surface exposed to OER through CV and CA shows a splitting value of 5.6 eV and 5.1 eV, respectively. A splitting of 5.6 eV indicates the presence of Mn_3O_4, while the splitting value of 5.1 eV can be attributed to a mixed oxidation state between +3 and +4.[21] The results indicate that the oxidation state of the MnO_x layer under CV and CA condition is different and slightly higher oxidation state is observed after CA experiment.

References

[1] I. Puigdomenech, *Chemical Equilibrium Diagrams*, `https://www.kth.se/che/medusa/`; `https://sites.google.com/site/chemdiagr/`; `https://github.com/ignasi-p/eq-diagr/`, 2018.

[2] N. Ingri, W. Kakolowicz, L. G. Sillén and B. Warnqvist, *Talanta*, 1967, **14**, 1261 – 1286.

[3] *Talanta*, 1968, **15**, xi – xii.

[4] G. Eriksson, *Anal. Chim. Acta*, 1979, **112**, 375 – 383.

[5] M. F. Al-Kuhaili, *J. Vac. Sci. Technol. A*, 2006, **24**, 1746–1750.

[6] S. Pishdadian and A. M. S. Ghaleno, *Acta Phys. Pol. A*, 2013, **123**, 741–745.

[7] N. Mironova-Ulmane, A. Kuzmin and M. Grube, *J. Alloys Compd.*, 2009, **480**, 97–99.

[8] Y. Mita, Y. Sakai, D. Izaki, M. Kobayashi, S. Endo and S. Mochizuki, *Phys. Status Solidi B*, 2001, **223**, 247–251.

[9] C. M. Julien, M. Massot and C. Poinsignon, *Spectrochim. Acta A*, 2004, **60**, 689–700.

[10] T. Gao, H. Fjellvåg and P. Norby, *Anal. Chim. Acta*, 2009, **648**, 235–239.

[11] C. Julien, M. Massot, S. Rangan, M. Lemal and D. Guyomard, *J. Raman Spectrosc.*, 2002, **33**, 223–228.

[12] T. Gao, H. Fjellvåg and P. Norby, *Nanotechnology*, 2009, **20**, 055610.

[13] E. S. Ilton, J. E. Post, P. J. Heaney, F. T. Ling and S. N. Kerisit, *Appl. Surf. Sci.*, 2016, **366**, 475–485.

[14] J. M. Cerrato, M. F. Hochella, W. R. Knocke, A. M. Dietrich and T. F. Cromer, *Environ. Sci. Technol.*, 2010, **44**, 5881–5886.

[15] M. Risch, K. A. Stoerzinger, B. Han, T. Z. Regier, D. Peak, S. Y. Sayed, C. Wei, Z. Xu and Y. Shao-Horn, *J. Phys. Chem. C*, 2017, **121**, 17682–17692.

[16] M. C. Biesinger, B. P. Payne, A. P. Grosvenor, L. W. Lau, A. R. Gerson and R. S. Smart, *Appl. Surf. Sci.*, 2011, **257**, 2717 – 2730.

[17] C. N. R. Rao, D. D. Sarma, S. Vasudevan, M. S. Hegde and T. J. Meuring, *Proc. R. Soc. London Ser. A*, 1979, **367**, 239–252.

[18] V. R. Galakhov, M. Demeter, S. Bartkowski, M. Neumann, N. A. Ovechkina, E. Z. Kurmaev, N. I. Lobachevskaya, Y. M. Mukovskii, J. Mitchell and D. L. Ederer, *Phys. Rev. B*, 2002, **65**, 113102.

[19] H. Antoni, W. Xia, J. Masa, W. Schuhmann and M. Muhler, *Phys. Chem. Chem. Phys.*, 2017, **19**, 18434–18442.

[20] M. F. Tesch, S. A. Bonke, T. E. Jones, M. N. Shaker, J. Xiao, K. Skorupska, R. Mom, J. Melder, P. Kurz, A. Knop-Gericke, R. Schlögl, R. K. Hocking and A. N. Simonov, *Angew. Chem.*, 2019, **131**, 3464–3470.

[21] M. Huynh, C. Shi, S. J. L. Billinge and D. G. Nocera, *J. Am. Chem. Soc.*, 2015, **137**, 14887–14904.